Conference Paper, Published Version

Mcilvenny, Jason; Williamson, B. J.; Macdowall, C.; Gleizon, P.; O'Hara Murray, R.

3D modelling of upwelling around a headland

Zur Verfügung gestellt in Kooperation mit/Provided in Cooperation with:
TELEMAC-MASCARET Core Group

3D modelling of upwelling around a headland

Mcilvenny[1], J., Williamson[1], B. J., Macdowall[1], C., Gleizon[1], P., O'Hara Murray, R.[2],

Jason.mcilvenny@uhi.ac.uk

[1]: Environmental Research Institute, North Highland College, University of the Highlands and Islands, United Kingdom
[2]: Marine Scotland Science, Scotland, UK

Abstract – **Using in situ field measurements and hydrodynamic modelling, this study investigated tidal features around a promontory headland on the United Kingdom mainland. Two acoustic instruments were bottom mounted over a period of 15 weeks and x-band radar data was collected periodically.**

Data showed complex hydrodynamics with an upwelling feature present producing vertical water velocities of up to 0.219 m/s. In association with the upwelling, a prominent surface feature was visible in x-band radar data which developed throughout the tidal cycle.

Data from the instruments was used to calibrate a hydrodynamic model developed using the TELEMAC modelling suite. Models of sufficient complexity are required to resolve fine-scale hydrodynamics associated with such features. Previous 3D models of this region have used 10 equal spaced vertical layers; however, it was found such a model is insufficient to model the vertical upwelling produced by this feature or its development throughout the tidal cycle.

By experiment, it was found 32 vertical layers with a non-equidistant layer spacing produced an upwelling feature similar to what is seen in the ADCP data and x-band data. Upwelling features such as this are important for foraging animals and headlands are also becoming a focus for renewable energy developments.

***Keywords*: Headland, tidal stream, seabird, modelling**

I. INTRODUCTION

The hydrodynamics of a large promontory headland in fast tidal currents are explored with in situ measurements and ground-truthed modelling. The objectives are firstly to calibrate the model to field data and secondly to characterise the hydrodynamics of a fast-moving tidal stream around a promontory headland. In particular, the aim is to understand upwelling observed in the field to better model complex hydrodynamics seen in areas of fast tidal stream, which are of importance to marine megafauna and increasingly of interest for marine renewable energy extraction.

Previously modelling of flow around headlands has aimed to understand the local consequences of sediment depositions, trapping of pollutants, nutrients and marine species distributions ([2],[17],[18],[19],[20],[21]). Such studies have shown eddies cause concentration of nutrients and modifications of the currents. Eddies move across a headland system, causing fluctuations in current speed and direction and a change in the energy density [20]. An increase in density of marine animal foraging has been found around headlands [21]. Upwelling is associated with headlands suggesting that the upwelling of nutrient-rich bottom waters supports life at the ocean's surface [22].

II. METHODS

A. Study site

The Pentland Firth is located between the north mainland of Scotland and the Orkney Islands (Figure 1). The firth is associated with strong tidal flows exceeding 4 m/s in places ([14]; [15]). Plots available in supplementary material show the distribution of currents during flood and ebb tide in the Pentland Firth and M2 amplitude and phase around northern Scotland. Dunnet Head is a promontory which extends approximately 4 km from the mainland into the Pentland Firth. Water velocities around the headland average 1 m/s with a maximum of 2.6 m/s (instrument data from this study). The seabed around the headland rapidly descends to depths of greater than 70 m.
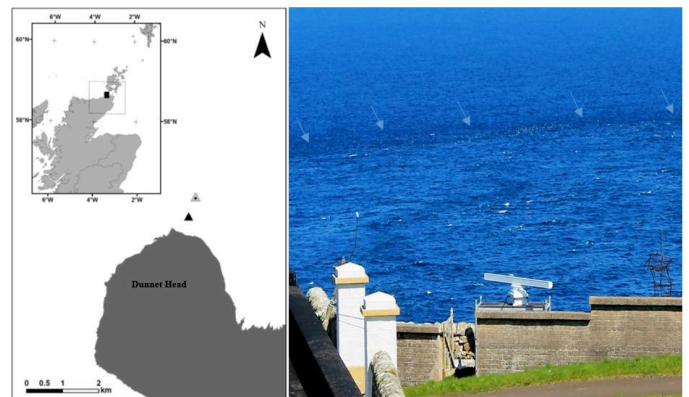

Figure 1. Map showing the location of the study area and model extent (insert) and location of ADCP (black triangle) and AWAC (grey triangle) instruments. Birds assembling along a linear surface feature (arrows) during flood tide. Photo taken from Dunnet Head lighthouse (58.67123◦ N, 3.37623◦ W).

B. Field Data

An ADCP (Acoustic Doppler Current Profiler) and a AWAC (Acoustic Wave and Current) were deployed of the tip of the headland for a period of 109 days between February and May 2018. The ADCP position was approximately 700 m north of the headland (58.67675◦ N, 3.36714◦ W) at 75 m depth. The AWAC was deployed further north, approximately 1.5 km to the north of Dunnet Head (58.68142◦ N, 3.36449◦ W) at approximately 89 m depth. The ADCP was programmed to record 10-min averages from an ensemble of 50 pings at a ping interval of 12 s. A total of 20 vertical bins were sampled, with a bin size of 4 m and a blanking distance of 1.76 m. The AWAC was programmed for 60 pings over a 10-min average with 44 bins, a bin size of 2 m and a 3 m blanking distance.

Post processing of the AWAC data was performed in Nortek STORM software with the removal of near surface bins (Bins 34–44). The AWAC was intermittently recording waves. In addition, a Nortek SeaDarQ X-Band radar system was deployed periodically at Dunnet Head overlooking the two instrument sites.

C. Model

The three-dimensional model was run using TELEMAC-3D (release version V8P0) using the non-hydrostatic version solving the Reynolds Averaged Navier-Stokes (RANS) equations in three directions. The model used the standard k-epsilon turbulence model in the horizontal and vertical directions and solved using the conjugate gradient solver for the linear systems. The N-Scheme for tidal flats was chosen as the advection scheme for the velocities and k-epsilon, The Nikurasde friction law was used (1.265). The TPXO tidal database for the European shelf was used for the tidal constituents.

The 3-D model used the fine-scale horizontal grid tested with the 2-D model using 50 m grid spacing in the proximity of Dunnet Head and 200 m spacing in the Pentland Firth channel with 2000 m spacing elsewhere and 500 m at the open-water boundaries. The time-step for the 3-D model was 5 s with 5-min interval model outputs. The 3-D model used differing vertical resolutions by altering the number of layers and spacing between layers. Increasing the number of layers results in greater accuracy; however, this increases computational time. In the TELEMAC-3D module options for defining equidistant spacing or non-equidistant spacing are controlled by the mesh transformation keyword and by defining levels in the USER_MESH_TRANSF subroutine.

Table I y+ mesh spacing for differing free stream velocities

Free stream velocity (m/s)	Wall spacing for y+ = 30 (m)	Wall spacing for y+ = 100 (m)	Wall spacing for y+ = 300 (m)
1	1.23	4.1	12.3
2	0.64	2.15	6.4
2.6	0.5	1.69	5
3	0.44	1.48	4.4

Models were run with 10, 16, and 32 layers with the number of layers chosen by using a value of 10 layers from earlier research ([23]; [24]; [25]; [26]) and from calculated y+ values (Table I). The y+ value is a non-dimensional distance to describe the required resolution of a mesh near bottom for a particular flow pattern. Values of $30 < y+ < 300$ have been suggested for the log law region to select the mesh spacing on the bottom ([27]). The log law, or law of the wall, states that the average velocity of a turbulent flow at a point is proportional to the logarithm of the distance from that point to the "wall", or the boundary of the fluid region ([28]). Boundary conditions on the bottom in TELEMAC-3D are, by default, an impermeable slip boundary; however, this can be changed to a no-slip condition provided the vertical mesh is refined at the bottom. This choice is valid if representing turbulence effects

due to the bottom, with bottom vertical resolution refined enough to model no-slip conditions. To investigate the effect of bottom boundary conditions on the 3-D model, three model runs were undertaken for distribution layers over the vertical for 10, 16 and 32-layer models with (a) equidistant layer spacing with log law boundary conditions, (b) non-equidistant layer spacing with a refined bottom using both log law and (c) no-slip boundary conditions. The first layer position was calculated using y+ = 30 for the non-equidistant cases.

III.   RESULTS

A. Field Data

Periods of high vertical velocity (w) are present during flood tides lasting between 1.5 and 3 h and are associated with the periods of high velocity error. ADCP vertical velocities reached a minimum of 0.206 m/s (downward) and maximum of 0.223 m/s (upward) with the dataset having a mean of the absolute values of 0.45 m/s and standard deviation of 0.028 m/s. The largest magnitude of vertical velocity occurs in Bin 7 of the ADCP data which equates to a mean depth of 46.7 m of a total mean water depth of 76.74 m with a tidal range of 5.08 m; however, vertical velocities > 0.50 m/s occur through all bins (Supplementary material). The data suggest there are periods of complex negative and positive vertical velocities during each flood tide (Figure 2). Similar vertical velocity spikes are seen in the AWAC data but have lower maximum and minimum velocities due to the AWAC position being further north of the headland. Frequency analysis of the AWAC vertical velocity shows a primary spike occurring at 0.4e-5 Hz or approximately 6 h using 15687 10-min samples. The ADCP data show a primary spike occurring at a frequency of 0.2e-5 Hz or approximately 12 h, and a secondary spike at a lower power occurring at approximately 6 h associated with the M2 and M4 tidal harmonics. Vertical velocity spikes exhibit a lag between the ADCP and AWAC data sets. Cross-correlation between the ADCP vertical velocity and AWAC showed 1.5 h in lag. This suggests a similar phenomenon affects the AWAC data later in the tidal phase than the ADCP. Increased periods of ADCP error velocity are associated with the same tidal phase, but error velocity is not strongly correlated with the vertical velocity increases, with a correlation coefficient of 0.14 with zero cross-correlation lag.
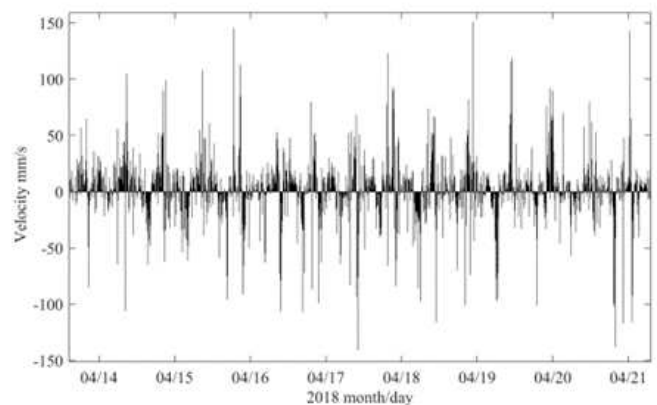

Figure 2. Bin 7 vertical velocities show velocity spikes of > 100 mm/s.

B. 3-D model

To address the complex hydrodynamics, a 3-D model was implemented to explore whether vertical velocities present in the ADCP data could be reproduced. Due to computational restrictions, a time period of increased vertical velocity activity was identified in the ADCP data for which 3-D model runs were undertaken. The 3-D model had an improved relationship with the field data, with a horizontal velocity RMSE of 0.22 for the AWAC position and 0.43 for the ADCP position with a 32-layer model using non-equidistant vertical layer spacing. The error between the model and the data is attributed to the lack of detail in the model in comparison with real variables (bathymetry, coastline shape, bottom type). The bathymetry used in the model is 1 arc second in resolution. However, the primary purpose of the 3-D model was to try to replicate the upwelling features and headland eddies.

Snapshots of the evolution of the vertical water velocity (w) were extracted from the 3-D model chosen to be presented here based on the ADCP data. (Figure 3).

1. Low water + 4 hours; 20/02/18 22:00. Initial formation of eddy during flood tide phase. Phase of negative vertical velocity indicated in ADCP data
2. Low water + 5 hours; 20/02/18 23:30; Mid flood tide
3. Low water + 6.5 hours; 21/02/18 01:00; Point at which maximum vertical velocities recorded in ADCP data. Towards end of flood tide phase.

These 3-time snapshots are extracted from each of the 10-layer, 16-layer and 32-layer models.

Figure 4. Vertical velocity (m/s) for model with 10 vertical layers, Time = Low water +4 h (x.1), +5 h (x.2) & +6.5 h (x.3) for plan slice at 37 m depth of (w) velocity for 3-D model with (1.x) equidistant vertical layers and log of the wall bottom boundary conditions. (2.x) non-equidistant vertical layers with log law boundary conditions with a first layer at height y+ = 30. (3.x) Non-equidistant layers with no-slip bottom conditions with first layer at y+ = 30. Black circles denote ADCP position (south) and AWAC position (north).
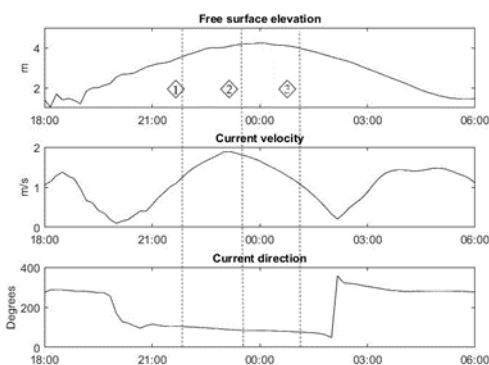
16-layer results

Figure 3. Free surface elevation (m) from 2-D model output, depth averaged current velocity (m/s) and depth averaged current direction (degrees) for from 20/02/18 to 21/02/18 showing time periods chosen (black diamonds, labels for dashed lines) for model snapshot outputs indicated by dashed lines.

10-layer Results

Snapshots from the 10-layer 3-D model for the three time phases (Figure 4) show increased vertical velocities at mid-depth are generated in the early stages of flood tide up to 0.12 m/s which dissipate early in the tidal cycle.
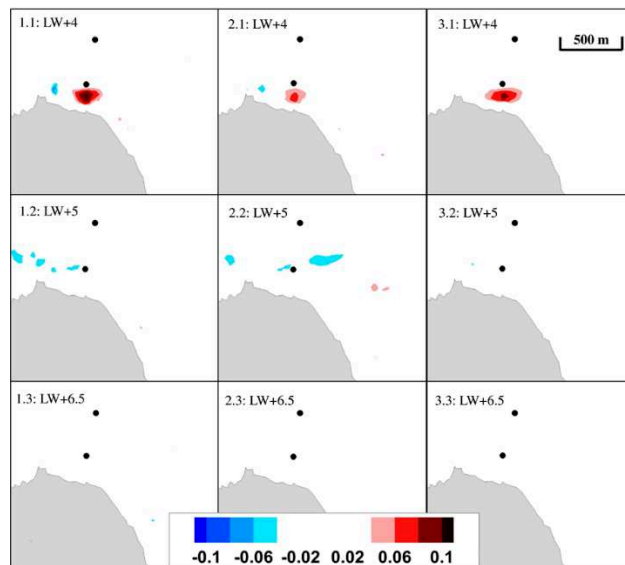

Figure 5. Vertical velocity (m/s) for model with 16 vertical layers, Time = Low water +4 h (x.1), +5 h (x.2) & +6.5 h (x.3) for plan slice at 37 m depth of (w) velocity for 3-D model with (1.x) equidistant vertical layers and log of the wall bottom boundary conditions. (2.x) non-equidistant vertical layers with log law boundary conditions with a first layer at height y+ = 30. (3.x) Non-equidistant layers with no-slip bottom conditions with first layer at y+ = 30. Black circles denote ADCP position (south) and AWAC position (north).

Results using 16 layers show extended evolution of the vertical velocities to low water + 5 hours and dissipation during low water + 6.5 hours. (Figure 5).

32-layer results

Model outputs using 32 layers show continued evolution of the region of increased vertical velocities through low water + 6.5 hours with most development in 2.3 (Figure 6). The vertical velocity reaches similar values as velocities present in the ADCP data during the same time interval (0.13 mm/s).
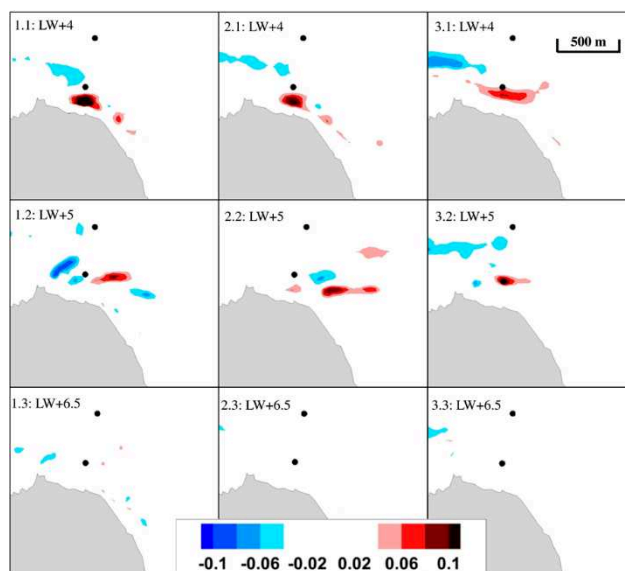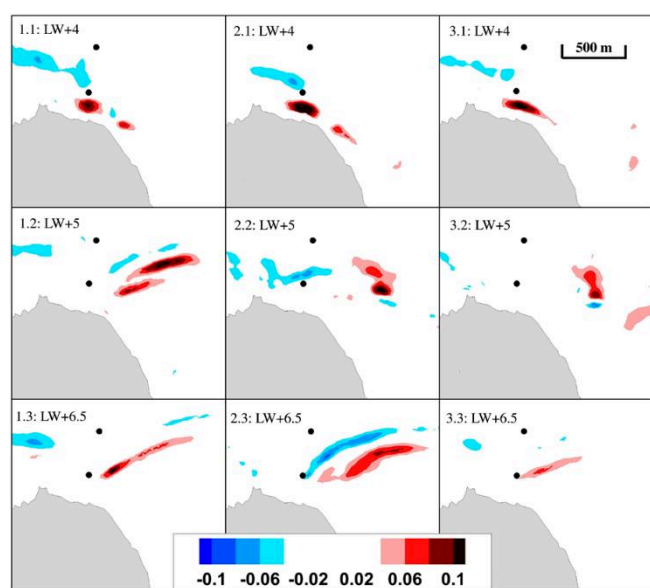

Figure 6. Vertical velocity (m/s) for model with 16 vertical layers, Time = Low water +4 h (x.1), +5 h (x.2) & +6.5 h (x.3) for plan slice at 37 m depth of (w) velocity for 3-D model with (1.x) equidistant vertical layers and log of the wall bottom boundary conditions. (2.x) non-equidistant vertical layers with log law boundary conditions with a first layer at height y+ = 30. (3.x) Non-equidistant layers with no-slip bottom conditions with first layer at y+ = 30. Black circles denote ADCP position (south) and AWAC position (north).

IV.   DISCUSSION

A linear surface feature is observed around a promontory headland which has been associated with observations of seabird foraging behaviour. Data from bottom-mounted instruments near this feature showed vertical velocity fluctuations modulated with tidal phase.

2-D and 3-D modelling was undertaken to replicate and understand the development of the features, in particular, the vertical velocity fluctuations seen in the ADCP data. Similar vertical upwelling was produced in a Telemac 3D model using 32 horizontal layers.

A. Field Data

The spikes of increased velocities in the instrument data and lag between the datasets is explained by the change of position of the tidal streak throughout the tidal phase, as the feature develops close to the headland and then moves offshore. For example, ADCP data show high vertical velocities are present at 01:00 on 21/02/2018 (low water + 6 hours). Later, the same spike in vertical velocities is seen in the AWAC data, with a lag of approximately 1.5 hours (low water + 7.5 hours). Vertical velocities of up to 0.219 m/s are recorded by the ADCP data for one 10-minute period. Mid-column velocities are used by other authors when reporting maximum vertical velocity from models ([29]; [30]).

Model results towards the end of flood tide (Low water + 6.5 h) closely resemble the timing of the spikes seen in the ADCP and AWAC data, where at approximately 02:30 on 21/02/18, increased vertical velocities are present in the AWAC data when the model indicated the movement of the area of increased vertical velocities outwards from the headland to the position of the AWAC (Figure 5). The frequency analysis between spikes in vertical velocity for the ADCP and AWAC are different; this is due to the instrument's position in relation to the ebb and tidal flood flow patterns and their relative positions to the headland tip upwelling and downwelling features.

Vertical velocity due to this type of secondary flow has been shown around other headlands. Vertical velocities of 8 mm/s around Cape Saunders, Otago, citing that upwelling caused the water column to be replaced by deeper waters in one tidal cycle [31]. Vertical velocities of 15 mm/s were measured around Rattray Island, Australia [30]. At Dunnet head, upwelling is stronger with the ADCP recording vertical speeds up to 0.223 m/s with a depth of 76.74 m, with the water column replacing itself every 5 minutes and 44 seconds under maximum upwelling conditions.

Strong secondary flow due to flow curvature around the tip of headlands and islands causes strong upwelling in the vicinity which can extend far downstream, where circulation normal to the main flow, the onshore flow near the bottom is drawn upwards and replaces the offshore transverse flow near the surface [30]. They found downwelling occurs with the reverse mechanism on the upstream side of the island and is highly localised and weaker than the upwelling. Here downwelling and upwelling are seen in the ADCP and AWAC data associated with the linear surface feature. This is also seen in the Telemac 3D results and likely a result of headland shape, bathymetry and strength of the tidal flow.

Four mechanisms for vertical motion were identified in previous research [30]; (a) where deficit in volume is larger near the surface than near the bottom, by continuity bottom water comes to surface to replace surface water, causing upwelling; (b) the opposite to this causing downwelling; (c) onshore flow similar to converging flow causing downwelling; (d) curved flows where there is a balance between centripetal acceleration based on the depth averaged velocity and the positive pressure gradient due to the tilting of the sea surface. This causes inward convergence of the bottom water which flows upwards within the water column. They state eddy and

tip upwelling can be encountered with varying magnitudes depending on the radius of curvature, flow intensity and surface pressure gradient. In the case of a study site at Rattray Island, bathymetry and topography of the island lead to the observed upwelling and downwelling present [30]. At Dunnet Head, flood water has a larger curve around the headland due to the flow approaching the Pentland Firth from the west. During ebb tide the flow is deflected prior to reaching Dunnet head by small islands in the firth to the east, causing less curvature. This may partially explain weaker upwelling and downwelling seen in the data during ebb tide; however, another cause of the weaker upwelling and downwelling during ebb tide is the instruments positions in relation to downstream upwelling and downwelling, whereby the instruments are in favourable positions to detect flood tide upwelling and downwelling. The depth, sharp bathymetric slope, flow curvature around Dunnet Head and high tidal current velocity provide the mechanisms for the strong vertical velocities seen in the data.

B. 3D model results

The 32-layer model using a refined bottom mesh with a first vertical layer at y+ = 30 and log law bottom boundary conditions produced results which resemble field data. Other model scenarios showed dissipation of this feature much earlier in the flood tide phase. Whilst the 32-layer, 50-m horizontal resolution, model may be improved upon, it was adequate to represent the field data and could be run on a desktop computer for short model runs of several days. Turbulent features probably have an impact the RANS equations do not accurately reproduce, in part due to the mesh resolution and the difference between horizontal and vertical mesh sizes. No-slip condition results with 32 layers and a refined bottom vertical mesh do not reproduce timings of vertical velocity as seen in field results. The model may not have enough vertical resolution for accurate no-slip conditions, and to do so would greatly increase computational requirements. The 32-layer model with log law bottom boundary conditions has better agreement with the data than an equidistant layer model, where a first layer position of y+ = 30 is a good solution for this flow with the k-epsilon turbulent closure model.

The 32-layer 3-D model produced a 300 m wide 2 km zone of upwelling and 100 m width 1.5 km zone of downwelling on the lee side of headland during flood tide with acceptable computational time, with similar characteristics observed in opportunistic X-band radar field data.

3-D modelling using 10 or 16 layers did not reproduce the extent of vertical velocities present in the instrument data. 3-D modelling using 32 layers and a refined bottom was sufficient to model the timing of the vertical velocity seen in the data but does not reproduce the magnitude of the velocities. However, 3-D modelling indicates the eddy system during flood tide is associated with a tidally induced linear upwelling/downwelling feature which provides explanation for the vertical velocity spikes in instrument field data and potentially explains observed seabird foraging behaviour in the vicinity of the streak feature.

Previous modelling in the Pentland Firth has used a range of vertical resolutions from 10 equidistant layers ([23]; [33]) to 20 layers ([32]). Previous research in the area used the Delft3-D-Flow model using the hydrostatic pressure assumption and 10 equidistant layers for sensitivity analysis of turbulent closure models [32]. In areas of complex hydrodynamics such as Dunnet Head, careful selection of horizontal layers and thickness of horizontal layers is required to model complex vertical movements.

V.   CONCLUSIONS

Dunnet Head is an extreme example of upwelling and downwelling associated with strong tidal flow and secondary flow due to flow curvature causing a noticeable surface feature. Vertical velocities of greater than 200 mm/s have been recorded by field instruments.

Initial observations (boat-based and cliff-based) indicate the study site is a preferred feeding location targeted by seabirds, with birds congregating and actively foraging along the surface expression of the tidal streak. As Dunnet Head is a nesting site for many seabirds, the tidal front may act as an important local feeding area affording the seabirds minimum energy to forage in the vicinity of the nesting site. Attraction of seabirds to the feature is likely a result of the hydrodynamic processes affecting prey, either concentrating them or making them more easily available near the surface and may be directly attributable to the vertical currents and turbulence associated with this feature.

The modelling work reproduces upwelling observed in the field and recorded by field instruments; however, models of sufficient complexity are required to resolve fine-scale hydrodynamics which are associated with such features, which is of importance to tidal stream renewable energy developments in these environments, as well as understanding foraging activity of marine top predators. Models using 32 vertical layers were sufficient to reproduce patterns of vertical velocities seen in field data. This study highlights that some areas, in particular headlands, may not be suitable for tidal energy developments due to the nature of the complex hydrodynamics due to secondary flow features, and potentially their importance for foraging megafauna.

Further work is proposed to investigate the role hydrodynamics plays regarding prey availability and the predictable presence and behaviour of foraging marine wildlife. Measuring velocities using a 5-beam ADCP combined with an echo sounder will allow investigation of the role turbulence and vertical currents play in biophysical associations of predators with hydrodynamic features, and changes to prey aggregation, disorientation and availability. Further surveys are planned to include vantage-point surveys for seabirds and marine mammals at Dunnet Head lighthouse and aerial surveys using a small unmanned aerial vehicle for combined biophysical data collection.

REFERENCES

[14] Goddijn-Murphy, L., Woolf, D.K., Easton, M.C., 2013. Current patterns in the inner sound (Pentland Firth) from underway ADCP data. J. Atmos. Ocean. Technol. 30, 96–111. https://doi.org/10.1175/JTECH-D-11-00223.1

[15] Neill, S.P., Vögler, A., Goward-Brown, A.J., Baston, S., Lewis, M.J., Gillibrand, P.A., Waldman, S., Woolf, D.K., 2017. The wave and tidal resource of Scotland. Renew. Energy 114, 3–17. https://doi.org/10.1016/j.renene.2017.03.027

[16] Signell, R.P. & Geyer, W.R. 1991. Transient eddy formation around headlands. J. Geophys. Res. Ocean. 96, 2561–2575. https://doi.org/10.1029/90jc02029J

[17] Davies, P.A., Dakin, J.M. & Falconer, R.A. 1995. Eddy formation behind a coastal headland. J. Coast. Res. 11, 154–167.

[18] Bastos, A., Collins, M. & Kenyon, N. 2003. Water and sediment movement around a coastal headland: Portland Bill, southern UK, in: Ocean Dynamics. 53, 309–321. https://doi.org/10.1007/s10236-003-0031-1

[19] McCabe, R.M., MacCready, P. & Pawlak, G. 2006. Form drag due to flow separation at a headland. J. Phys. Oceanogr. 36, 2136–2152. https://doi.org/10.1175/JPO2966.1

[20] Lin, J., Lin, B., Sun, J. & Chen, Y. 2017. Numerical model simulation of island-headland induced eddies in a site for tidal current energy extraction. Renew. Energy 101, 204–213. https://doi.org/10.1016/j.renene.2016.08.055

[21] Waggitt, J.J., Cazenave, P.W., Torres, R., Williamson, B.J. & Scott, B.E. 2016. Predictable hydrodynamic conditions explain temporal variations in the density of benthic foraging seabirds in a tidal stream environment. ICES J. Mar. Sci. 73, 2677–2686. https://doi.org/10.1093/icesjms/fsw100

[22] Russell, P. & Vennell, R. 2017. High-resolution observations of secondary circulation and tidally synchronized upwelling around a coastal headland, J. Geophys. Res. Oceans, 122, 890–913, doi:10.1002/2016JC012117.

[23] Rahman, A., Venugopal, V., 2015. Inter-comparison of 3D tidal flow models applied to Orkney islands and pentland firth. In: 11th European Wave and Tidal Energy Conference (EWTEC).

[24] Chatzirodou, A., Karunarathna, H. & Reeve, D.E. 2017. Modelling 3D hydrodynamics governing island-associated sandbanks in a proposed tidal stream energy site. Appl. Ocean Res. 66, 79–94. https://doi.org/10.1016/j.apor.2017.04.008

[25] Stansby, P., Chini, N. & Lloyd, P. 2016. Oscillatory flows around a headland by 3D modelling with hydrostatic pressure and implicit bed shear stress comparing with experiment and depth-averaged modelling. Coast. Eng. 116, 1–14. https://doi.org/10.1016/j.coastaleng.2016.05.008

[26] Waldman, S., Bastón, S., Nemalidinne, R., Chatzirodou, A., Venugopal, V. & Side, J. 2017. Implementation of tidal turbines in MIKE 3 and Delft3D models of Pentland Firth & Orkney Waters. Ocean Coast. Manag. 147, 21–36. https://doi.org/10.1016/j.ocecoaman.2017.04.015

[27] Salim, S.M. & Cheah, S.C., 2009. Wall y+ Strategy for Dealing with Wall-bounded Turbulent Flows, in: International Multi Conference of Engineers and Computer Scientists, IMECS 2009, Hong Kong.

[28] Chanson, H., 2009. Applied Hydrodynamics: an Introduction to Ideal and Real Fluid Flows. CRC Press. https://doi.org/10.1201/b11464.

[29] Alaee, M.J., Ivey, G. & Pattiaratchi, C. 2004. Secondary circulation induced by flow curvature and Coriolis effects around headlands and islands. Ocean Dyn. 54, 27–38. https://doi.org/10.1007/s10236-003-0058-3

[30] White, L., Wolanski, E., 2008. Flow separation and vertical motions in a tidal flow interacting with a shallow-water island. Estuarine, Coastal and Shelf Science 77, 457-466.

[31] Russell, P. & Vennell, R. 2009. Observations of secondary flow and upwelling at Cape Saunders, Otago Peninsula. Proceedings Australasian Coasts and Ports conference, Wellington Sept 2009.

[32] Baston, S., Harris, R.E., Woolf, D.K., Hiley, R.A. & Side, J.C. 2013. Sensitivity Analysis of the Turbulence Closure Models in the Assessment of Tidal Energy Resource in Orkney. EWTEC 2013 Proc. https://doi.org/10.13140/2.1.3033.3762

[33] O'Hara Murray, R. & Gallego, A. 2017. A modelling study of the tidal stream resource of the Pentland Firth, Scotland. Renew. Energy 102, 326–340. https://doi.org/10.1016/j.renene.2016.10.053